Quantum graphs: a simple model for chaotic scattering

2003 J. Phys. A: Math. Gen. 36 3501

(http://iopscience.iop.org/0305-4470/36/12/337)

INSTITUTE OF PHYSICS PUBLISHING JOURNAL OF PHYSICS A: MATHEMATICAL AND GENERAL

J. Phys. A: Math. Gen. **36** (2003) 3501–3524 PII: S0305-4470(03)40053-X

Quantum graphs: a simple model for chaotic scattering

Tsampikos Kottos[1] **and Uzy Smilansky**[2]

[1] Max-Planck-Institut für Strömungsforschung, 37073 Göttingen, Germany
[2] Department of Physics of Complex Systems, The Weizmann Institute of Science, 76100 Rehovot, Israel

E-mail: tsamp@chaos.gwdg.de

Received 26 July 2002, in final form 27 September 2002
Published 12 March 2003
Online at stacks.iop.org/JPhysA/36/3501

Abstract

We connect quantum graphs with infinite leads, and turn them into scattering systems. We show that they display all the features which characterize quantum scattering systems with an underlying classical chaotic dynamics: typical poles, delay time and conductance distributions, Ericson fluctuations, and when considered statistically, the ensemble of scattering matrices reproduces quite well the predictions of the appropriately defined random matrix ensembles. The underlying classical dynamics can be defined, and it provides important parameters which are needed for the quantum theory. In particular, we derive exact expressions for the scattering matrix, and an exact trace formula for the density of resonances, in terms of classical orbits, analogous to the semiclassical theory of chaotic scattering. We use this in order to investigate the origin of the connection between random matrix theory and the underlying classical chaotic dynamics. Being an exact theory, and due to its relative simplicity, it offers new insights into this problem which is at the forefront of the research in chaotic scattering and related fields.

PACS numbers: 05.45.Mt, 03.65.Nk, 02.10.Yn

1. Introduction

Quantum graphs of one-dimensional wires connected at nodes had already been introduced more than half a century ago to model physical systems. Depending on the envisaged application the precise formulation of the models can be quite diverse and ranges from solid-state applications to mathematical physics [1–12]. Lately, quantum graphs have also attracted the interest of the quantum chaos community because they can be viewed as typical and yet relatively simple examples for the large class of systems in which classically chaotic dynamics implies universal correlations in the semiclassical limit [13–21]. Up to now we have only a

limited understanding of the reasons for this universality, and quantum graph models provide a valuable opportunity for mathematically rigorous investigations of the phenomenon. In particular, for quantum graphs an exact trace formula exists [12–14] which is based on the periodic orbits of a mixing classical dynamical system. Moreover, it is possible to express the two-point spectral correlation functions in terms of purely combinatorial problems [16–19].

By attaching infinite leads at the vertices, we get non-compact graphs, for which a scattering theory can be constructed [22–24]. They display many of the features that characterize scattering systems with an underlying chaotic classical dynamics [25–29], and they are the subject of this paper. The *quantum* scattering matrix for such problems can be written explicitly, together with a trace formula for the density of its resonances. These expressions are the analogues of the corresponding semiclassical approximations available in the theory of chaotic scattering [25–27], albeit here they are exact. With these tools we analyse the distribution of resonances, partial delay times, and the statistics of the fluctuating scattering amplitudes and cross sections. Moreover, we address issues such as the statistical properties of the ensemble of the scattering matrices, and conductance distribution. Finally, we analyse the effect of non-uniform connectivity on the statistical properties of the scattering matrix. A main part of our analysis will be focused on the comparison of the statistical properties of the above quantities with the random matrix theory (RMT) predictions [30–40].

The paper is structured in the following way. In section 2, the mathematical model is introduced and the main definitions are given. Section 3 is devoted to the derivation of the scattering matrix for graphs. The trace formula for the density of resonances of quantum graphs is presented in section 4 which includes also the analysis of the underlying classical system. The next section is dedicated to the analysis of various statistical properties of the S-matrix. Our numerical data are compared both with the predictions of RMT and with the semiclassical expectations. Finally, in section 6, we analyse the class of star graphs for which several results can be analytically derived. Our conclusions are summarized in section 7.

2. Quantum graphs: definitions

We start by considering a *compact* graph $\mathcal{G}$. It consists of V *vertices* connected by B *bonds*. The number of bonds which emanate from each vertex i defines the valency v_i of the corresponding vertex (for simplicity we will allow only a single bond between any two vertices). The graph is called v*-regular* if all the vertices have the same valency v. The total number of bonds is $B = \frac{1}{2}\sum_{i=1}^{V} v_i$. Associated with every graph is its connectivity matrix C. It is a square matrix of size V whose matrix elements $C_{i,j}$ take the values 1 if the vertices i, j are connected with a bond, or 0 otherwise. The bond connecting the vertices i and j is denoted by $b \equiv (i, j)$, and we use the convention that $i < j$. It will sometimes be convenient to use the 'time-reversed' notation, where the first index is the larger, and $\hat{b} \equiv (j, i)$ with $j > i$. We shall also use the directed bonds representation, in which b and $\hat{b}$ are distinguished as two directed bonds conjugated by time reversal. We associate the natural metric with the bonds, so that $x_{i,j}$ ($x_{j,i}$) measures the distance from the vertex i (j) along the bond. The lengths of the bonds are denoted by L_b and we shall henceforth assume that they are *rationally independent*. The mean length is defined by $\langle L\rangle \equiv (1/B)\sum_{b=1}^{B} L_b$ and in all numerical calculations below it will be taken to be 1. In the *directed-bond* notation $L_b = L_{\hat{b}}$.

The *scattering* graph $\tilde{\mathcal{G}}$ is obtained by adding leads which extend from M ($\leqslant V$) vertices to infinity. For simplicity we connect at most one lead to any vertex. The valency of these vertices increases to $\tilde{v}_i = v_i + 1$. The M leads are denoted by the index i of the vertex to which they are attached while x_i now measures the distance from the vertex along the lead i.

The Schrödinger operator (with $\hbar = 2m = 1$) is defined on the graph $\tilde{\mathcal{G}}$ in the following way: on the bonds b, the components Ψ_b of the total wavefunction Ψ are solutions of the one-dimensional equation

$$\left(-\mathrm{i}\frac{\mathrm{d}}{\mathrm{d}x} - A_b\right)^2 \Psi_b(x) = k^2 \Psi_b(x) \qquad b = (i, j) \tag{1}$$

where A_b (with $\mathrm{Re}(A_b) \neq 0$ and $A_b = -A_{\hat{b}}$) is a 'magnetic vector potential' which breaks the time-reversal symmetry. In most applications we shall assume that all the A_b are equal and the bond index will be dropped. The components of the wavefunctions on the leads, $\Psi_i(x)$, are solutions of

$$-\frac{\mathrm{d}^2}{\mathrm{d}x^2}\Psi_i(x) = k^2 \Psi_i(x) \qquad i = 1, \ldots, M. \tag{2}$$

At the vertices, the wavefunction satisfies boundary conditions which ensure current conservation. To implement the boundary conditions, the components of the wavefunction on each of the bonds b and the leads i are expressed in terms of counter propagating waves with a wave vector k:

$$\begin{aligned} &\text{on the bonds: } \Psi_b = a_b\, \mathrm{e}^{\mathrm{i}(k+A_b)x_b} + c_b\, \mathrm{e}^{\mathrm{i}(-k+A_b)x_b} \\ &\text{on the leads: } \Psi_i = I_i\, \mathrm{e}^{-\mathrm{i}kx_i} + O_i\, \mathrm{e}^{ikx_i}. \end{aligned} \tag{3}$$

The amplitudes a_b, c_b on the bonds and I_i, O_i on the lead are related by

$$\begin{pmatrix} O_i \\ a_{i,j_1} \\ \cdot \\ a_{i,j_{v_i}} \end{pmatrix} = \Sigma^{(i)} \begin{pmatrix} I_i \\ c_{j_1,i} \\ \cdot \\ c_{j_{v_i},i} \end{pmatrix}; \qquad \Sigma^{(i)} = \begin{pmatrix} \rho^{(i)} & \tau^{(i)}_{j_1} & \cdot & \tau^{(i)}_{j_{v_i}} \\ \tau^{(i)}_{j_1} & \tilde{\sigma}^{(i)}_{j_1,j_1} & \cdot & \tilde{\sigma}^{(i)}_{j_1,j_{v_i}} \\ \cdot & \cdot & \cdot & \cdot \\ \tau^{(i)}_{j_{v_i}} & \tilde{\sigma}^{(i)}_{j_{v_i},j_1} & \cdot & \tilde{\sigma}^{(i)}_{j_{v_i},j_{v_i}} \end{pmatrix}. \tag{4}$$

These equalities impose the boundary conditions at the vertices. The vertex scattering matrices $\Sigma^{(i)}_{j,j'}$, are $\tilde{v}_i \times \tilde{v}_i$ unitary symmetric matrices, and j, j' go over all the v_i bonds and the lead which emanate from i. The unitarity of $\Sigma^{(i)}$ guarantees current conservation at each vertex.

On the right-hand side of (4), the vertex scattering matrix $\Sigma^{(i)}$ was written explicitly in terms of the vertex reflection amplitude $\rho^{(i)}$, the lead–bond transmission amplitudes $\left\{\tau^{(i)}_j\right\}$, and the $v_i \times v_i$ bond–bond transition matrix $\tilde{\sigma}^{(i)}_{j,j'}$, which is *sub-unitary* ($|\det \tilde{\sigma}^{(i)}| < 1$), due to the coupling to the leads.

Graphs for which there are no further requirements on the $\Sigma^{(i)}$ shall be referred to as *generic*. It is often convenient to compute the vertex scattering matrix from a requirement that the wavefunction is continuous and satisfies *Neumann* boundary conditions at that vertex [13, 14]. These graphs shall be referred to as Neumann graphs, and the resulting $\tilde{\Sigma}^{(i)}$ matrices read [22]:

$$\tilde{\sigma}^{(i)}_{j,j'} = \frac{2}{\tilde{v}} - \delta_{j,j'}; \qquad \tau^{(i)}_j = \frac{2}{\tilde{v}}; \qquad \rho^{(i)} = \frac{2}{\tilde{v}} - 1. \tag{5}$$

Vertices which are not coupled to leads have $\rho^i = 1, \tau^{(i)}_j = 0$, while the bond–bond transition matrix $\tilde{\sigma}^{(i)}_{j.j'} = \frac{2}{v} - \delta_{j,j'}$ is unitary.

3. The *S*-matrix for quantum graphs

It is convenient to first discuss graphs with leads connected to all the vertices $M = V$. The generalization to an arbitrary number $M \leqslant V$ of leads (channels) is straightforward and will be presented at the end of this section.

To derive the scattering matrix, we first write the bond wavefunctions using the two representations which are conjugated by 'time reversal':

$$\begin{aligned}\Psi_b(x_b) &= a_b\,\mathrm{e}^{\mathrm{i}(k+A_b)x_b} + c_b\,\mathrm{e}^{\mathrm{i}(-k+A_b)x_b}\\ \Psi_{\hat{b}}(x_{\hat{b}}) &= a_{\hat{b}}\,\mathrm{e}^{\mathrm{i}(k+A_{\hat{b}})x_{\hat{b}}} + c_{\hat{b}}\,\mathrm{e}^{\mathrm{i}(-k+A_{\hat{b}})x_{\hat{b}}}\\ &= a_{\hat{b}}\,\mathrm{e}^{\mathrm{i}(-k-A_{\hat{b}})x_b}\,\mathrm{e}^{\mathrm{i}(k+A_{\hat{b}})L_b} + c_{\hat{b}}\,\mathrm{e}^{\mathrm{i}(-k+A_{\hat{b}})L_b}\,\mathrm{e}^{\mathrm{i}(k-A_{\hat{b}})x_b}.\end{aligned} \tag{6}$$

Hence,

$$c_b = a_{\hat{b}}\,\mathrm{e}^{\mathrm{i}(k+A_{\hat{b}})L_b} \qquad a_b = c_{\hat{b}}\,\mathrm{e}^{\mathrm{i}(-k+A_{\hat{b}})L_b}. \tag{7}$$

In other words, except for a phase factor, the outgoing wave from the vertex i in the direction j is identical to the incoming wave at j coming from i.

Substituting a_b from equation (7) in equation (4), and solving for $c_{i,j}$ we get

$$c_{i,j'} = \sum_{r,s}(\mathbf{1} - \tilde{S}_B(k;A))^{-1}_{(i,r),(s,j)} D_{(s,j)}\tau_s^{(j)} I_j \qquad O_i = \rho^{(i)} I_i + \sum_{j'} \tau_{j'}^{(i)} c_{ij'} \tag{8}$$

where $\mathbf{1}$ is the $2B \times 2B$ unit matrix. Here, the 'bond scattering matrix' $\tilde{S}_b$ is a sub-unitary matrix in the $2B$-dimensional space of directed bonds which propagates the wavefunctions. It is defined as $\tilde{S}_B(k, A) = D(k; A)\tilde{R}$, with

$$D_{ij,i'j'}(k, A) = \delta_{i,i'}\delta_{j,j'}\,\mathrm{e}^{\mathrm{i}kL_{ij}+\mathrm{i}A_{i,j}L_{ij}} \qquad \tilde{R}_{ji,nm} = \delta_{n,i}C_{j,i}C_{i,m}\tilde{\sigma}^{(i)}_{ji,im}. \tag{9}$$

$D(k, A)$ is a diagonal unitary matrix which depends only on the metric properties of the graph, and provides a phase which is due to free propagation on the bonds. The sub-unitary matrix $\tilde{R}$ depends on the connectivity and on the bond–bond transition matrices $\tilde{\sigma}$. It assigns a scattering amplitude for transitions between connected directed bonds. $\tilde{R}$ is sub-unitary, since

$$|\det \tilde{R}| = \prod_{i=1}^{V} |\det \tilde{\sigma}^{(i)}| < 1. \tag{10}$$

Replacing $c_{i,j'}$ in the second of equations (8), we get the following relation between the outgoing and incoming amplitudes O_i and I_j on the leads:

$$O_i = \rho^{(i)} I_i + \sum_{j'jrs} \tau_{j'}^{(i)}(\mathbf{1} - \tilde{S}_B(k;A))^{-1}_{(i,r),(s,j)} D_{(s,j)}\tau_s^{(j)} I_j. \tag{11}$$

Combining (11) for all leads $i = 1, \ldots, V$, we obtain the unitary $V \times V$ scattering matrix $S^{(V)}$,

$$S^{(V)}_{i,j} = \delta_{i,j}\rho^{(i)} + \sum_{r,s} \tau_r^{(i)}(\mathbf{1} - \tilde{S}_B(k;A))^{-1}_{(i,r),(s,j)} D_{(s,j)}\tau_s^{(j)}. \tag{12}$$

Finally, a multiple scattering expansion for the S-matrix is obtained by substituting

$$(\mathbf{1} - \tilde{S}_B(k;A))^{-1} = \sum_{n=0}^{\infty} \tilde{S}_B^n(k;A) \tag{13}$$

into equation (12). The expansion (13) converges absolutely on the real k-axis since for generic graphs the spectrum of $\tilde{S}$ is strictly inside the unit circle (or else, for $k + \mathrm{i}\epsilon$, with $\epsilon > 0$ arbitrarily small).

The scattering matrix can be decomposed into two parts $S^{(V)}(k) = \langle S^{(V)}\rangle_k + S^{fl}(k)$ which are associated with two well-separated time scales of the scattering process. $\langle S^{(V)}\rangle_k$ can be evaluated by averaging term by term the S-matrix resulting from the substitution of the multiple scattering expansion (13) in (12). Since all terms, except for the prompt reflections, are oscillatory functions of k, they average to zero (we assume that the k-window over which

the averaging is performed is sufficiently large, i.e. larger than $2\pi/L_{\min}$) and thus we get that $\langle S^{(V)}\rangle_k = S^D = \delta_{i,j}\rho^i$. The fluctuating component of the S-matrix, $S^{fl}(k)$, starts by a transmission from the incoming lead i to the bonds (i, r) with transmission amplitudes $\tau_r^{(i)}$. The wave gains a phase $\mathrm{e}^{\mathrm{i}(k+A_b)L_b}$ for each bond it traverses and a scattering amplitude $\tilde{\sigma}_{r,s}^{(i)}$ at each vertex. Eventually, the wave is transmitted from the bond (s, j) to the lead j with an amplitude $\tau_s^{(j)}$. Explicitly,

$$S_{i,j}^{(V)} = \delta_{i,j}\rho^{(i)} + \sum_{t\in\mathcal{T}_{i\to j}} \mathcal{B}_t\, \mathrm{e}^{\mathrm{i}(kl_t+\Theta_t)} \tag{14}$$

where $\mathcal{T}_{i\to j}$ is the set of trajectories on $\tilde{\mathcal{G}}$ which lead from i to j. $\mathcal{B}_t$ is the amplitude corresponding to a path t whose length and directed length are $l_t = \sum_{b\in t} L_b$ and $\Theta_t = \sum_{b\in t} L_b A_b$, respectively. Thus the scattering amplitude $S_{i,j}^{(V)}$ is a sum of a large number of partial amplitudes, whose complex interference brings about the typical irregular fluctuations of $\left|S_{i,j}^{(V)}\right|^2$ as a function of k.

One of the basic concepts in the quantum theory of scattering are the resonances. They represent long-lived intermediate states to which bound states of a closed system are converted due to coupling to continua. On a formal level, resonances show up as poles of the scattering matrix $S^{(M)}$ occurring at complex wave numbers $\kappa_n = k_n - \frac{\mathrm{i}}{2}\Gamma_n$, where k_n and Γ_n are the position and width of the resonances, respectively. From (12) it follows that the resonances are the complex zeros of

$$\zeta_{\tilde{\mathcal{G}}}(\kappa) = \det(\mathbf{1} - \tilde{S}_B(\kappa; A)) = 0. \tag{15}$$

The eigenvalues of $\tilde{S}_B$ are in the unit circle, and therefore the resonances appear in the lower half of the complex κ plane. Moreover from equation (15) it is clear that their formation is closely related to the internal dynamics inside the scattering region which is governed by $\tilde{S}_B$.

There exists an intimate link between the scattering matrix and the spectrum of the corresponding closed graph. It manifests the exterior–interior duality [41] for graphs. The spectrum of the closed graph is the set of wave numbers for which $S^{(V)}$ has +1 as an eigenvalue. This corresponds to a solution where no currents flow in the leads so that the conservation of current is satisfied on the internal bonds. 1 is in the spectrum of $S^{(V)}$ if

$$\zeta_{\mathcal{G}}(k) = \det[\mathbf{1} - S^{(V)}(k)] = 0. \tag{16}$$

Equation (16) can be transformed in an alternative form

$$\zeta_{\mathcal{G}}(k) = \det[\mathbf{1} - \rho]\frac{\det[\mathbf{1} - D(k)R]}{\det[\mathbf{1} - D(k)\tilde{R}]} = 0 \qquad R_{i,r;s,j} = \tilde{R}_{i,r;s,j} + \delta_{r,s}\frac{\tau_i^{(r)}\tau_j^{(r)}}{1-\rho^{(r)}} \tag{17}$$

which is satisfied once

$$\det[\mathbf{1} - D(k)R] = 0. \tag{18}$$

In contrast to $\tilde{R}$, R is a unitary matrix in the space of directed bonds, and therefore the spectrum is real. Equation (18) is the secular equation for the spectrum of the compact part of the graph, and it was derived in a different way in [13].

The difference $\delta R = R - \tilde{R}$ gets smaller as larger graphs are considered (for graphs with Neumann boundary conditions it is easy to see that the difference is of order $\frac{1}{v}$). That is, the leads are weakly coupled to the compact part of the graph, and one can use perturbation theory for the computation of the resonance parameters. To lowest order, ($\delta R = 0$), the resonances coincide with the spectrum of the compact graph. Let k_n be in the spectrum. Hence, there exists a vector $|n\rangle$ which satisfies the equation

$$D(k_n)R|n\rangle = 1|n\rangle. \tag{19}$$

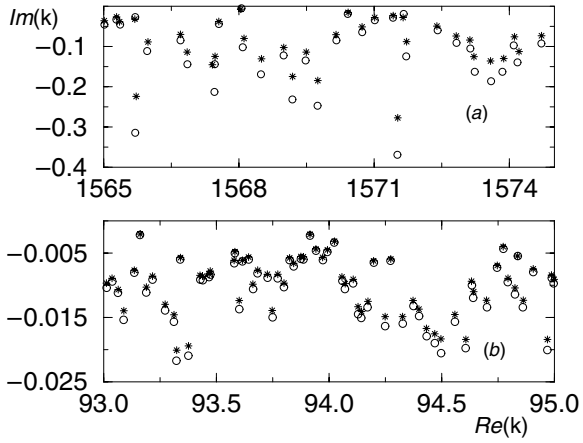

Figure 1. Poles of the $S^{(V)}$-matrix for regular Neumann graphs. The exact evaluated poles are indicated with ($\circ$) while ($*$) are the results of the perturbation theory (20): (*a*) $V = 5$ and $v = 4$ and (*b*) $V = 15$ and $v = 14$.

To first order in δR, the resonances acquire a width

$$\delta\kappa_n = -\mathrm{i}\frac{\langle n|D(k_n)\delta R|n\rangle}{\langle n|L|n\rangle}. \tag{20}$$

To check the usefulness of this result, we searched numerically for the true poles for a few scattering graphs and compared them with the approximation (20). In figure 1, we show the comparison for fully connected Neumann graphs with $V = 5$, 15 and $A = 0$. As expected the agreement between the exact poles and the perturbative results improves as v increases.

We finally comment that the above formalism can be easily modified for graphs where not all the vertices are attached to leads. If the vertex l is not attached, one has to set $\rho^{(l)} = 1$, $\tau_j^{(l)} = 0$ in the definition of $\Sigma^{(l)}$. The dimension of the scattering matrix is then changed accordingly.

For the sake of completeness we quote here an alternative expression for the S-matrix which applies for Neumann graphs, exclusively [14, 24]. For this purpose, we define the $V \times V$ matrix

$$h_{i,j}(k, A) = \begin{cases} -\sum_{m\neq i} C_{i,m}\cot(kL_{i,m}) & i = j \\ C_{i,j}\,\mathrm{e}^{-\mathrm{i}A_{i,j}L_{i,j}}(\sin(kL_{i,j}))^{-1} & i \neq j \end{cases} \tag{21}$$

in terms of which,

$$S^{(V)} = (\mathrm{i}\mathbf{1} + h(k))^{-1}(\mathrm{i}\mathbf{1} - h(k)) \tag{22}$$

where $\mathbf{1}$ is the $V \times V$ unit matrix. $S^{(V)}$ is unitary since $h(k)$ is Hermitian.

In the case of graphs connected to leads at an arbitrary set of $M < V$ vertices with indices $\{i_l\}$, $l = 1, \ldots, M$, the $M \times M$ scattering matrix $S^{(M)}$ has to be modified in the following way:

$$S^{(M)} = 2\mathrm{i}W(h(k) + \mathrm{i}W^T W)^{-1}W^T - \mathbf{1}. \tag{23}$$

Here $W_{i_l,j} = \delta_{i_l,j}$ is the $M \times V$ leads–vertices coupling matrix ($W = \mathbf{1}$ when $M = V$). This form of the S-matrix is reminiscent of the expression which was introduced by Weidenmüller to generalize the Breit–Wigner theory for many channels and internal states. However, (23) is an exact expression which involves no truncations.

It follows from (23) that in the present case, one can identify the poles of the S-matrix with the zeros of

$$\zeta_{\mathcal{G}}(\kappa) = \det(h(\kappa) + \mathrm{i}W^T W) = 0. \tag{24}$$

Its main advantage over (15) is that it involves a determinant of a matrix of much lower dimension.

4. The trace formula for resonances and classical scattering on graphs

In the spectral theory of bounded Hamiltonian systems, the most fundamental object of study is the spectral density which consists of a sum of δ functions at the spectral points. For open systems, it is replaced by the resonance density, which is defined on the real k line and consists of an infinite sum of Lorentzians which are centred at $k_n = \mathrm{Re}\,\kappa_n$ and have width $\Gamma_n = -2\,\mathrm{Im}\,\kappa_n$, where κ_n are the complex poles of the scattering matrix. In this section, we shall express the resonance density for scattering graphs in terms of periodic orbits of their compact part. This is the analogue of the trace formula for bounded graphs.

4.1. The trace formula

The resonance density $d_R(k)$ can be deduced from the total phase $\Phi(k) = \frac{1}{\mathrm{i}} \ln \det S^{(M)}(k)$ of the scattering matrix [43]:

$$d_R(k) \equiv \frac{1}{2\pi}\frac{\mathrm{d}\Phi}{\mathrm{d}k} = -\mathrm{i}\frac{1}{2\pi}\frac{\partial}{\partial k} \ln \det S^{(M)}(k). \tag{25}$$

It is a smooth function for real k, and can be interpreted as the mean length of the *delay* associated with the scattering at wave number k [26].

Using equation (12) and performing standard manipulations [42], we obtain the following expression for the phase $\Phi(k)$:

$$\Phi(k) - \Phi(0) = -2\,\mathrm{Im}\,\ln\det(I - \tilde{S}_B(k; A)) + \mathcal{L}k \tag{26}$$

where $\mathcal{L} = 2\sum_{b=1}^{B} L_b$ is twice the total length of the bonds of $\tilde{\mathcal{G}}$.

Using the expansion

$$\ln\det(I - \tilde{S}_B(k; A)) = -\sum_{n=1}^{\infty} \frac{1}{n} \mathrm{Tr}\,\tilde{S}_B^n(k; A) \tag{27}$$

we rewrite equation (26) as

$$\Phi(k) = \Phi(0) + \mathcal{L}k + 2\,\mathrm{Im}\sum_{n=1}^{\infty} \frac{1}{n} \mathrm{Tr}\,\tilde{S}_B^n(k; A). \tag{28}$$

On the other hand, using equation (9) we can write $\mathrm{Tr}\,\tilde{S}_B^n(k; A)$ as sums over n-periodic orbits on the graph

$$\mathrm{Tr}\left(\tilde{S}_B^n(k; A)\right) = \sum_{p\in\mathcal{P}_n} n_p \tilde{\mathcal{A}}_p^r\, \mathrm{e}^{\mathrm{i}(l_p k + \Theta_p)r} \tag{29}$$

where the sum is over the set $\mathcal{P}_n$ of primitive periodic orbits whose period n_p is a divisor of n, with $r = n/n_p$ (primitive periodic orbits are those which cannot be written as a repetition of a shorter periodic orbit). The amplitudes $\tilde{\mathcal{A}}_p$ are the products of the bond–bond scattering amplitudes $\tilde{\sigma}^{(i)}_{b,b'}$ along the primitive loops, i.e.

$$\tilde{\mathcal{A}}_p = \prod_{i=1}^{n_p} \tilde{\sigma}^{(i)}_{b,b'}. \tag{30}$$

Substituting equations (28) and (29) in equation (25) one gets the resonance density

$$d_R(k) = \frac{1}{2\pi}\mathcal{L} + \frac{1}{\pi}\,\mathrm{Re}\sum_{n=1}^{\infty}\sum_{p\in\mathcal{P}_n} n_p l_p r \tilde{\mathcal{A}}_p^r\, \mathrm{e}^{\mathrm{i}(l_p k+\Theta_p)r} \tag{31}$$

Equation (31) is an *exact* trace formula for the resonance density. The first term on the right-hand side of equation (31) corresponds to the smooth resonance density, while the second provides the fluctuating part. We note that the mean resonance spacing is given by

$$\Delta = \frac{2\pi}{\mathcal{L}} \simeq \frac{2\pi}{2B\langle L\rangle} \tag{32}$$

and it is the same as the mean level spacing obtained for the corresponding bounded graph $\mathcal{G}$ [12, 13].

4.2. Classical dynamics

We conclude this section with a discussion of the classical dynamics on the graph $\tilde{\mathcal{G}}$. A classical particle moves freely as long as it is on a bond. The vertices are singular points, and it is not possible to write down the analogue of the Newton equations there. In [13, 14] it was shown that it is possible to define a classical evolution on the graph: a *Poincaré section* on the graph consists of the discrete set of directed bonds. The phase-space density at a (topological) time n is the set of occupation probabilities $\rho_b(n)$ of the directed bonds, and the classical evolution is governed by a Markovian master equation. Applied to the compact part of a scattering graph it reads

$$\tilde{\rho}_b(n+1) = \sum_{b'} \tilde{U}_{b,b'}\tilde{\rho}_{b'}(n) \tag{33}$$

where the transition matrix $\tilde{U}_{b,b'}$ is given by the corresponding *quantum* transition probability

$$\tilde{U}_{ij,nm} = |\tilde{R}_{ij,nm}|^2 = \delta_{j,n}\left|\sigma^{(j)}_{ij,jm}\right|^2. \tag{34}$$

Note that $\tilde{U}$ does not involve any metric information on the graph.

Due to loss of flux to the leads $\sum_{b'}\tilde{U}_{bb'} < 1$, and the phase-space measure is not preserved, but rather, decays in time. The probability to remain on $\tilde{\mathcal{G}}$ is

$$\tilde{P}(n) \equiv \sum_{b=1}^{2B}\rho_b(n) = \sum_{b,b'}\tilde{U}_{bb'}\rho_{b'}(n-1) \simeq \mathrm{e}^{-\Gamma_{cl}n}\tilde{P}(0) \tag{35}$$

where $\exp(-\Gamma_{cl})$ is the largest eigenvalue of the 'leaky' evolution operator $\tilde{U}_{bb'}$.

For the v-regular graph with $\tilde{\sigma}^{(i)}$ given by (5) the spectrum of $\tilde{U}$ is restricted to the interior of a circle with radius given by the maximum eigenvalue $\nu_1 = (v-1)\tau^2+\rho^2$ with the corresponding eigenvector $|1\rangle = (1/2B)(1,1,\ldots,1)^T$. Hence the decay rate $\Gamma_{cl} = -\ln\nu_1$ for regular Neumann graphs take the simple form

$$\Gamma_{cl} = -\ln(1-\tau^2) \approx (2/(1+v))^2. \tag{36}$$

We note that removing the leads from the vertices and turning $\tilde{\mathcal{G}}$ into a compact graph $\mathcal{G}$ we get $\Gamma_{cl} = 0$ since in this case $\tau^{(i)} = 0$ (and $\rho^{(i)} = 1$) and the phase-space measure is preserved as expected.

The inverse decay rate $T_{cl} = \Gamma_{cl}^{-1}$, gives the average classical delay time that the particle spends within the interaction region. Injecting a particle from the leads to the scattering domain, its probability of being on any bond randomizes, because at each vertex a Markovian choice of one out of v directions is made. The longer a particle remains within the interaction regime, the more scattering events it experiences. The set of trapped trajectories whose occupancy decays exponentially in time is the analogue of the strange repeller in generic Hamiltonian systems displaying 'chaotic scattering'.

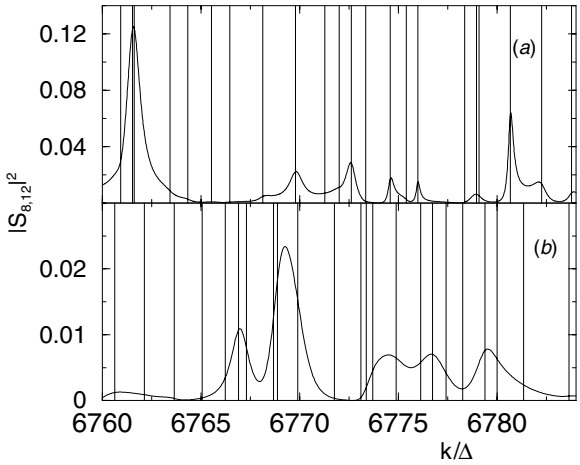

Figure 2. Representative examples of scattering cross sections $|S_{i,j}^{(V)}|^2$ for Neumann graphs in a regime of (*a*) isolated resonances ($V = 15$, $v = 14$ with corresponding $\langle\gamma\rangle_k = 0.59$) and (*b*) overlapping resonances ($V = 49$, $v = 14$ with corresponding $\langle\gamma\rangle_k \simeq 2$). The real parts of the resonances in this energy interval are indicated by the vertical lines.

5. Statistical analysis of the *S*-matrix

So far we have developed the scattering theory of graphs, pointing out their similarity with scattering systems which display chaotic scattering in the classical limit. Due to the interference of a large number of amplitudes, the S-matrix fluctuates as a function of k, and its further analysis calls for a statistical approach which will be the subject of this section. We shall show that quantum graphs possess typical poles, delay time and conductance distributions, Ericson fluctuations of the scattering amplitudes, and when considered statistically, the ensemble of scattering matrices is very well reproduced by the predictions of RMT. At the same time deviations from the universal RMT results, which are related to the system-specific properties of some graphs, will be pointed out. The study of these deviations is especially convenient for graphs because of the transparent and simple scattering theory developed in terms of scattering trajectories.

An important parameter which is associated with the statistical properties of the S-matrix is the Ericson parameter defined through the scaled mean resonance width as

$$\langle\gamma\rangle_k \equiv \frac{\langle\Gamma_n\rangle_k}{\Delta} \tag{37}$$

where $\langle\cdot\rangle_k$ denotes spectral averaging and Δ is the mean spacing between resonances. The Ericson parameter determines whether the resonances overlap ($\langle\gamma\rangle_k > 1$) or are isolated ($\langle\gamma\rangle_k < 1$). Typical examples for the two extreme situations are shown in figure 2.

The degree of resonance overlap determines the statistical properties of the S-matrix. We shall show in the following that the mean width can be approximated by the classical decay rate $\langle\gamma\rangle_k = \gamma_{cl}$. For the v-regular graphs discussed above, we have

$$\gamma_{cl} \equiv \frac{\Gamma_{cl}}{\Delta} \approx \frac{4}{2\pi}\frac{v}{1+v}\frac{V}{1+v} \tag{38}$$

where we made use of equations (32) and (36). Thus changing v and V we can control the degree of overlap allowing us to test various phenomena.

In what follows, unless explicitly specified, we shall consider regular graphs with one lead attached to each vertex, i.e. $M = V$. Finally, the widths are always scaled by the mean spacing Δ, i.e. $\gamma_n \equiv \frac{\Gamma_n}{\Delta}$.

5.1. The resonance width distribution

The resonance width distribution can be computed for a given graph in the following way. Consider the complex $\kappa = x + \mathrm{i}y$ plane, where the zeros of the secular function

$$\zeta_{\tilde{\mathcal{G}}}(\kappa) = \det(\mathbf{1} - \tilde{S}_B(\kappa; A)) = f(x, y) + \mathrm{i}g(x, y) \tag{39}$$

are the poles of the S-matrix (resonances). The variables (x, y) are expressed in units of Δ. On average, the number of resonances with real part, $x \in [0, X]$ is X. The density of resonance widths reads

$$\mathcal{P}(\gamma) = \lim_{X\to\infty} \frac{1}{X} \int_0^X \delta(f(x, y = -\gamma))\delta(g(x, y = -\gamma)) \left| \frac{\mathrm{d}\zeta_{\tilde{\mathcal{G}}}(\kappa)}{\mathrm{d}\kappa} \right|^2_{y=-\gamma} \mathrm{d}x. \tag{40}$$

We used the Cauchy–Riemann theorem for the evaluation of the Jacobian $(f_x g_y - f_y g_x)$ which multiplies the two δ functions that locate the complex zeros of $\zeta_{\tilde{\mathcal{G}}}$. We now recall that the κ dependence of $\tilde{S}_B(\kappa; A)$ comes from the factors $\mathrm{e}^{\mathrm{i}\kappa L_b}$ in (9). This implies that for a given y, $\zeta_{\tilde{\mathcal{G}}}$ is a quasi-periodic function of x. Moreover, expanding the determinant (39) it is not difficult to show that the frequencies involved can be written as linear combinations of the bond lengths $\lambda = \sum q_b L_b$ with integer coefficients $q_b = 0, 1$ or 2. Since the bond lengths are rationally independent, we find that $\zeta_{\tilde{\mathcal{G}}}$ depends on a *finite* number of incommensurate frequencies. Expression (40) can be regarded as a 'time' integral over a trajectory on a multidimensional incommensurate torus, which covers the torus ergodically. Hence, the integral can be replaced by a phase-space average,

$$\mathcal{P}(\gamma) = \int_0^{2\pi} \frac{\mathrm{d}\psi_1}{2\pi} \cdots \int_0^{2\pi} \frac{\mathrm{d}\psi_J}{2\pi} \delta(f(\vec{\psi}, -\gamma))\delta(g(\vec{\psi}, -\gamma)) \left| \frac{\mathrm{d}\zeta_{\tilde{\mathcal{G}}}(\vec{\psi}, -\gamma)}{\mathrm{d}\kappa} \right|^2. \tag{41}$$

Here $\vec{\psi}$ denotes the vector of independent angles on the J-dimensional torus. Although the above formula provides a general framework, its application to actual graphs is a formidable task.

An important feature of the distribution of the resonances in the complex plane can be deduced by studying the secular function $\zeta_{\tilde{\mathcal{G}}}(\kappa)$. Consider $\zeta_{\tilde{\mathcal{G}}}(\kappa = 0)$. If one of the eigenvalues of the matrix $\tilde{R}$ (9) takes the value 1, $\zeta_{\tilde{\mathcal{G}}}(k = 0) = 0$ and because of the quasi-periodicity of $\zeta_{\tilde{\mathcal{G}}}$, its zeros reach any vicinity of the real axis infinitely many times. The largest eigenvalue of the $\tilde{R}$-matrix for v-regular Neumann graphs is 1, and therefore the distribution of resonance widths is finite in the vicinity of $\gamma = 0$. For generic graphs, the spectrum of $\tilde{R}$ is inside a circle of radius $\lambda_{\max} < 1$. This implies that the poles are excluded from a strip just under the real axis, whose width can be estimated by

$$\Gamma_{\mathrm{gap}} = -2\ln(|\lambda_{\max}|)/L_{\max} \tag{42}$$

where $L_{\max}$ is the maximum bond length. The existence of a gap is an important feature of the resonance width distribution $\mathcal{P}(\gamma)$ for chaotic scattering systems.

A similar argument was used recently in [23] in order to obtain an *upper* bound for the resonance widths. It is

$$\Gamma_{\max} \sim -2\ln(|\lambda_{\min}|)/L_{\min} \tag{43}$$

where $\lambda_{\min}$ and $L_{\min}$ are the minimum eigenvalue and bond length, respectively.

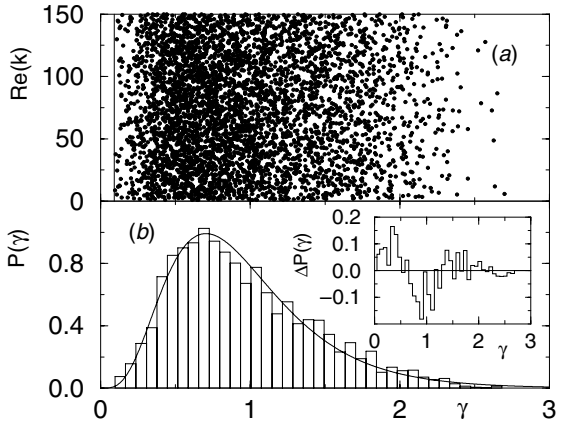

Figure 3. (*a*) The 5000 resonances of a single realization of a complete $V = 5$ graph with $A \neq 0$ and $M = V$. The solid line marks the position of the gap γ_{gap}. (*b*) The distribution of resonance widths $\mathcal{P}(\gamma)$. The solid line is the RMT prediction (45). The difference $\mathcal{P}(\gamma) - \mathcal{P}_{CUE}(\gamma)$ is shown in the inset.

The distribution of the complex poles for a generic fully connected graph with $V = 5$ is shown in figure 3(*a*). The vertical line which marks the region from which resonances are excluded was computed using (42).

Random matrix theory can provide an expression for the distribution of resonances. In the case of non-overlapping resonances, perturbation theory shows that the resonance widths are distributed according to the so-called χ^2 distribution

$$\mathcal{P}(\gamma) = \frac{(\beta M/2)^{\beta M/2}}{\langle\gamma\rangle_k \Gamma(\beta M/2)} \left(\frac{\gamma}{\langle\gamma\rangle_k}\right)^{\beta M/2-1} \exp(-\gamma\beta M/2\langle\gamma\rangle_k) \tag{44}$$

where $\beta = 1$ (2) for systems which respect (break) time-reversal symmetry, and $\Gamma(x)$ is the gamma-function. Once $\langle\gamma\rangle_k$ becomes large enough the resonances start to overlap, and (44) does not hold. In the general case, Fyodorov and Sommers [36, 37] proved that the distribution of scaled resonance widths for the unitary random matrix ensemble is given by

$$\mathcal{P}(\gamma) = \frac{(-1)^M}{\Gamma(M)} \gamma^{M-1} \frac{\mathrm{d}^M}{\mathrm{d}\gamma^M} \left(\mathrm{e}^{-\gamma\pi g} \frac{\sinh(\gamma\pi)}{(\gamma\pi)}\right) \tag{45}$$

where the parameter $g = \frac{2}{\left(1-\langle S^D\rangle_k^2\right)} - 1$ controls the degree of coupling with the channels (and it is assumed that $g_i = g\ \forall i = 1, \ldots, M$). For $g \gg 1$ (i.e. weak coupling regime) equation (45) reduces to (44).

In the limit of $M \gg 1$, equation (45) reduces to the following expression [37]:

$$\mathcal{P}(\gamma) = \begin{cases} \dfrac{M}{2\pi\gamma^2} & \text{for} \quad \dfrac{M}{\pi(g+1)} < \gamma < \dfrac{M}{\pi(g-1)} \\ 0 & \text{otherwise} \end{cases}. \tag{46}$$

It shows that in the limit of large number of channels there exists a strip in the complex κ plane which is free of resonances. This is in agreement with previous findings [27, 30, 44]. In the case of maximal coupling, i.e. $g = 1$, the power law (46) extends to infinity, leading to divergences of the various moments of γ. Using (45) we recover the well-known Moldauer–Simonius relation [30] for the mean resonance width [37]

$$\langle\gamma\rangle_k = -\frac{\sum_{i=1}^{V} \ln(|\langle S^D\rangle_k|^2)}{2\pi}. \tag{47}$$

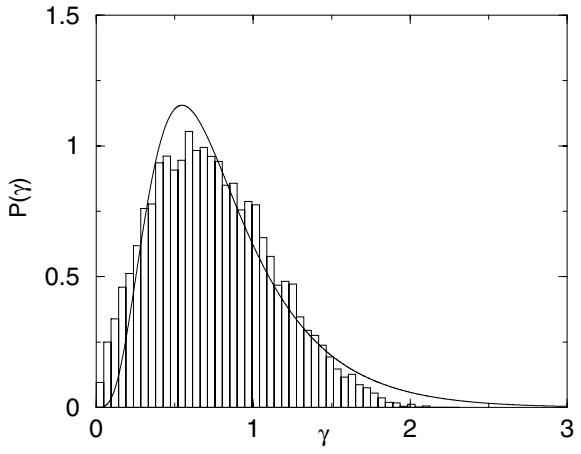

Figure 4. Resonance width distribution $\mathcal{P}(\gamma)$ for a complete Neumann graph with $M = V = 5$ and $A \neq 0$. The solid line is the RMT prediction (45).

The resonance width distribution for a $V = 5$ regular and generic graph is shown in figure 3(b) together with the RMT prediction, which reproduces the numerical distribution quite well. Figure 4 shows a similar comparison for a Neumann graph. In this case, a clear deviation from the RMT prediction is observed. The main feature of $\mathcal{P}(\gamma)$ is the relatively high abundance of resonances in the vicinity of the real axis which is of dynamical nature and conforms with the expectations (see related discussion above equation (42)).

5.2. The form factor

To investigate further the dynamical origin of the resonance fluctuations, we study the resonance two-point form factor $K(t)$. The main advantage of $K(t)$ is that it allows us to study the resonance fluctuations in terms of classical orbits. It is defined as

$$K_R(t) \equiv \int \mathrm{d}\chi \, \mathrm{e}^{\mathrm{i}2\pi\chi\mathcal{L}t} R_2(\chi) \tag{48}$$

where t measures lengths in units of the Heisenberg length $l_H = \mathcal{L}$ and $R_2(\chi)$ is the excess probability density of finding two resonances at a distance χ,

$$R_2(\chi; k_0) = \left\langle \tilde{d}_R\left(k + \frac{\chi}{2}\right) \tilde{d}_R\left(k - \frac{\chi}{2}\right) \right\rangle_k = \left\langle \frac{\Delta}{2k_0} \int_{-k_0}^{k_0} \tilde{d}_R\left(k + \frac{\chi}{2}\right) \tilde{d}_R\left(k - \frac{\chi}{2}\right) \mathrm{d}k \right\rangle_{k_0}. \tag{49}$$

Above $\langle \cdots \rangle_{k_0}$ indicates averaging over a number of spectral intervals of size $\Delta_k = 2k_0$, centred around k_0. Here $\tilde{d}_R(k)$ is the oscillatory part of $d_R(k)$ (see equation (31)). Substituting the latter in equations (48) and (49) we obtain $K_R(t)$ in terms of periodic orbits and their repetitions

$$K_R(t) = \frac{2\mathcal{N}}{\mathcal{L}^2} \left| \sum_p \sum_r l_p \tilde{\mathcal{A}}_p^r \, \mathrm{e}^{\mathrm{i}(kl_a + \Theta_a)} \delta_{\mathcal{N}}(t - r l_p/\mathcal{L}) \right|^2 \tag{50}$$

where $\delta_{\mathcal{N}}(x) = (\sin(\mathcal{N}x/2))/(\mathcal{N}x/2)$ and $\mathcal{N} = \frac{\Delta_k}{\Delta}$. A similar sum contributes to the spectral form factor of the compact graph [13, 14]. However, the corresponding amplitudes are different due to the fact that $\tilde{\mathcal{A}}_p$ also contains the information about the escape of flux to the leads.

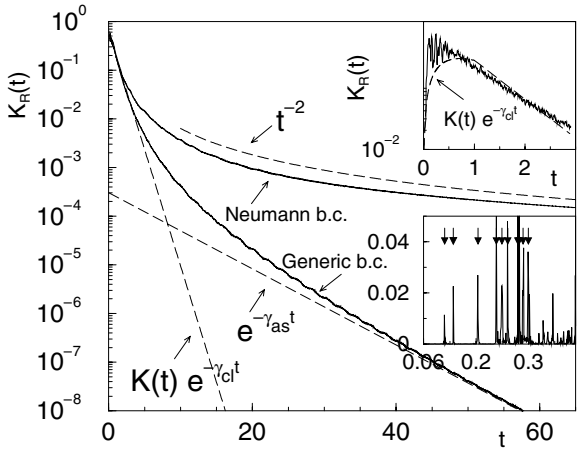

Figure 5. The form factors $K_R(t)$ for a complete $V = 5$ graph, with either generic or Neumann boundary conditions, $A \neq 0$ and $M = V$. The data were averaged over 5000 spectral intervals and smoothed on small t intervals. Upper inset: $K_R(t)$ for small times. The solid line corresponds to the numerical data for the pentagon with generic boundary conditions while the dashed line is the approximant $K_R(t) \approx K(t)\exp(-\gamma_{cl}t)$. Lower inset: $K_R(t)$ calculated with high resolution. The lengths of periodic orbits of the closed graph are indicated by arrows.

Assuming that all periodic orbits decay at the same rate, one would substitute $\tilde{\mathcal{A}}_p$ with $\mathcal{A}_p \exp(-n_p\gamma_{cl}/2)$ where $\mathcal{A}_p$ is the weight assigned to the periodic orbit of the corresponding closed system. Then equation (50) takes the following simple form:

$$K_R(t) \approx K(t)\, \mathrm{e}^{-\gamma_{cl}t} \tag{51}$$

where $K(t)$ is the form factor of the compact system [29]. Note that for $t \ll \gamma_{cl}^{-1}$ the resonance form factor $K_R(t)$ is equal to $K(t)$. This is reasonable since an open system cannot be distinguished from a closed one during short times. This simple approximation is checked in the inset of figure 5 (see dashed line) and it is shown to reproduce the numerical data rather well in the domain $t \leqslant 5$. The asymptotic decay is dominated by the resonances which are nearest to the gap, and it cannot be captured by the crude argument presented above. For a generic graph, K_R decays exponentially but with a rate given by $\gamma_{as} = \gamma_{\mathrm{gap}}$ (the best fit, indicated in figure 5 by the dashed line, gives γ_{as} which agrees with γ_{gap} within 30%). For the graph with Neumann boundary conditions, $\gamma_{\mathrm{gap}} = 0$ and one expects an asymptotic power-law decay. The corresponding best fit (see dashed line in figure 5) shows t^{-2}.

In Hamiltonian systems in more than one dimension, the size of the spectral interval Δ_k where the spectral average is performed is limited by the requirement that the smooth part of the spectral density is approximately constant. Here, instead we can take arbitrarily large spectral intervals since the smooth spectral density is constant [13, 14]. This way, one can reach the domain where the function $K_R(t)$ is composed of arbitrarily sharp spikes which completely resolve the length spectrum for lengths which are both smaller and larger than l_H. In the inset of figure 5 we show the numerical $K(t)$ calculated with high enough resolution. In the same inset we mark with arrows the location of the lengths of short periodic orbits. We note that as long as $t\mathcal{L}$ is shorter than the length of the shortest periodic orbit, $K(t) = 0$. With increasing t, the periodic orbits become exponentially dense and therefore the peaks start to overlap, giving rise to a quasi-continuum described approximately by equation (51).

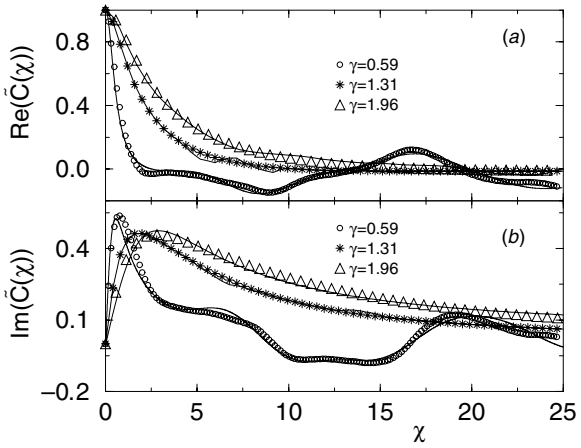

Figure 6. The autocorrelation function $\tilde{C}(\chi, \nu = 1)$ for regular graphs with Neumann boundary conditions. ($\circ$) correspond to a graph with $\gamma = 0.59$ (isolated resonance regime), ($*$) to a graph with $\gamma = 1.36$ (intermediate regime) and ($\triangle$) to a graph with $\gamma \simeq 2$ (overlapping resonances regime). The solid lines correspond to the theoretical expression (53): (*a*) The real part of $\tilde{C}(\chi, \nu = 1)$; (*b*) The imaginary part of $\tilde{C}(\chi, \nu = 1)$.

5.3. Ericson fluctuations

As was mentioned above, the scattering cross sections are dominated by either isolated resonances, or by overlapping resonances whose fluctuations follow a typical pattern. These patterns were first discussed by Ericson [45] in the frame of nuclear physics and were shown to be one of the main attributes of chaotic scattering [26]. The transition between the two regimes is controlled by the Ericson parameter (37). Typical fluctuating cross sections are shown in figure 2.

A convenient measure for Ericson fluctuations is the autocorrelation function

$$C(\chi;\nu) = \frac{1}{\Delta j}\sum_{j=j_{\min}}^{j_{\max}}\left(\left\langle S^{(M)}_{j,j+\nu}\left(k+\frac{\chi}{2}\right)S^{(M)\star}_{j,j+\nu}\left(k-\frac{\chi}{2}\right)\right\rangle_k - \langle S_{j,j+\nu}\rangle_k\langle S^{\star}_{j,j+\nu}\rangle_k\right) \tag{52}$$

where an additional average over $\Delta j = j_{\max} - j_{\min} + 1$ elements of the same scattering matrix was introduced for better statistical processing. To evaluate equation (52) we substitute the expression of the S-matrix from equation (14) and split the sum over trajectories into two distinct parts: the contributions of short trajectories are computed explicitly by following the multiple scattering expansion up to trajectories of length $l_{\max}$. The contributions of longer orbits are approximated by using the diagonal approximation, which results in a Lorentzian with a width $\gamma_{\rm Er}$. Including explicitly up to $n = 3$ scattering events we get,

$$C(\chi;\nu) \approx G\mathrm{e}^{\mathrm{i}l_{\max}\chi}\frac{\gamma_{\rm Er}}{\gamma_{\rm Er}-\mathrm{i}\chi} + \frac{1}{\Delta j}\sum_{j=j_{\min}}^{j_{\max}}\left[\tau^4\,\mathrm{e}^{\mathrm{i}\chi L_{j,j+\nu}} + \tau^4\rho^4\,\mathrm{e}^{3\mathrm{i}\chi L_{j,j+\nu}} + \tau^6\sum_{m\neq j,j+\nu}\mathrm{e}^{\mathrm{i}\chi(L_{j,m}+L_{m,j+\nu})}\right] \tag{53}$$

where G is determined by the condition $C(\chi = 0;\nu) = 1$. The interplay between the contributions of long and short periodic orbits is shown in figure 6 where we report the real and the imaginary parts of the scaled autocorrelation function $\tilde{C}(\chi) = C(\chi)/\mathrm{Re}[C(0)]$

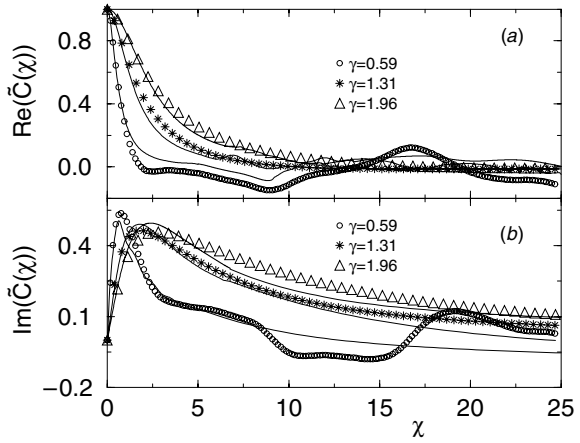

Figure 7. The autocorrelation function $\tilde{C}(\chi, \nu = 1)$ for the same graphs as in figure 6. The solid lines correspond to the RMT predictions [46]: (*a*) The real part of $\tilde{C}(\chi, \nu = 1)$; (*b*) The imaginary part of $\tilde{C}(\chi, \nu = 1)$.

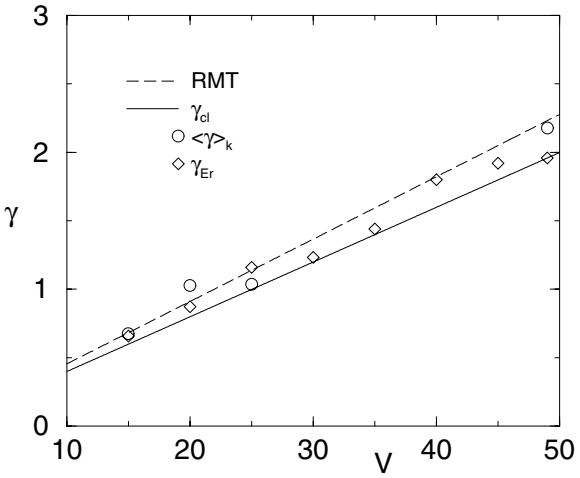

Figure 8. The mean resonance width $\langle\gamma\rangle_k$, autocorrelation width $\gamma_{\rm Er}$, the classical expectation γ_{cl} and the RMT prediction (47) versus V for various graphs with Neumann boundary conditions and constant valency $v = 14$.

separately. For overlapping resonances, the autocorrelation function is well reproduced by a Lorentzian while for the case of isolated resonances one can clearly see the contributions of short paths. In figure 7, we present the same numerical data for $\tilde{C}(\chi)$ together with the RMT predictions [46]. One can clearly see that although for small χ we have a relative good agreement between our numerical data and the RMT predictions, for $\tilde{C}(\chi)$, there are considerable deviations for large values of the argument χ. This is due to the existence of short trajectories which are system specific and therefore cannot be captured by the universal RMT results.

In figure 8, we report the mean resonance width $\langle\gamma\rangle_k$ calculated numerically for various graphs, the parameter $\gamma_{\rm Er}$ extracted from the best fit of the numerical $C(\chi)$ with equation (53), together with the RMT prediction equation (47) and the classical expectation

given by equation (38). The results justify the use of the classical estimate especially in the limit $V \to \infty$ for fixed v/V (which is the analogue of the semiclassical limit). In this limit, the RMT and the classical estimates coincide.

5.4. S-matrix statistics

One can further check the applicability of RMT by studying the entire $S^{(M)}$-matrix distribution function. The probability density of $M \times M$ unitary $S^{(M)}$-matrices is defined in a $M + \beta M(M-1)/2$ parameter space and was found first in [31] to be given by the Poisson kernel

$$\mathrm{d}\mathcal{P}_{\bar{S}}(S^{(M)}) = p_{\bar{S}}(S)\,\mathrm{d}\mu(S) = C_\beta \frac{[\det(1-\bar{S}\bar{S}^\dagger)]^{(\beta M+2-\beta)/2}}{|\det(1-\bar{S}\bar{S}^\dagger)|^{(\beta M+2-\beta)}}\,\mathrm{d}\mu_\beta(S) \tag{54}$$

where C_β is a normalization constant which depends on the symmetry class. All system-specific relevant information are included in the ensemble average $S^{(M)}$-matrix, defined as $\bar{S}_{i,j} = \langle S^D \rangle_k$. For regular graphs, $\bar{S}$ is proportional to the unit matrix, i.e. $\bar{S}_{i,j} = \frac{1-v}{1+v}\delta_{i,j}$, while the eigenvectors are distributed uniformly and independently of the eigenphases. The invariant measure $\mathrm{d}\mu_\beta(S)$ is given as

$$\mathrm{d}\mu_\beta(S^{(M)}) = \prod_{i<j} |\mathrm{e}^{\mathrm{i}\phi_i} - \mathrm{e}^{\mathrm{i}\phi_j}|^\beta \prod_{i=1}^{M} \mathrm{d}\phi_i\,\mathrm{d}\Omega \tag{55}$$

where $\mathrm{d}\Omega$ is the solid angle on the M-dimensional unit hypersphere.

For large M values, a numerical check of this probability distribution is prohibitive. However, for $M = 2$ one can easily find the exact form of (54) and compare it with the numerical results. The resulting distribution of the eigenphases ϕ_1, ϕ_2 of the 2×2 scattering matrices of regular graphs is given by

$$\mathrm{d}\mathcal{P}_{\bar{S}}(S^{(2)}) = \frac{C_\beta \left(\frac{4v}{(v+1)^2}\right)^{\beta+2} \sin^\beta\left(\frac{\omega}{2}\right)}{\left[1 - 4\bar{S}\cos\left(\frac{\omega}{2}\right)\cos\psi + 2\bar{S}^2\left(2\cos^2\left(\frac{\omega}{2}\right) + \cos(2\psi)\right) - 4\bar{S}^3\cos\psi\cos\left(\frac{\omega}{2}\right) + \bar{S}^4\right]^{\frac{\beta+2}{2}}}\,\mathrm{d}\omega\,\mathrm{d}\psi \tag{56}$$

where we used the notation $\psi = \frac{\phi_1+\phi_2}{2}$ and $\omega = \phi_1 - \phi_2$. Integrating equation (56) over ω, ψ we get the corresponding distribution functions $\mathcal{P}_{\bar{S}}(\omega)$ and $\mathcal{P}_{\bar{S}}(\psi)$. Our numerical results for an ensemble of S-matrices calculated for different realizations of the lengths of the graphs are reported in figure 9 together with the RMT predictions (56) for a regular graph with two channels. An overall good agreement is seen both for $A = 0$ and $A \neq 0$.

5.5. Partial delay times statistics

The Wigner delay time captures the time-dependent aspects of quantum scattering. It can be interpreted as the typical time for which an almost monochromatic wave packet remains in the interaction region. It is defined as

$$T_W = \frac{1}{2\mathrm{i}M}\,\mathrm{Tr}\left[S^{(M)\dagger}\frac{\mathrm{d}S^{(M)}(k)}{\mathrm{d}k}\right] = \frac{1}{2M}\sum_{i=1}^{M}\frac{\partial\phi_i(k)}{\partial k} \tag{57}$$

where ϕ_i are the eigenphases of the $S^{(M)}$-matrix. The partial derivatives $\frac{\partial\phi_i(k)}{\partial k}$ are the *partial delay times* and their statistical properties were studied extensively within the RMT

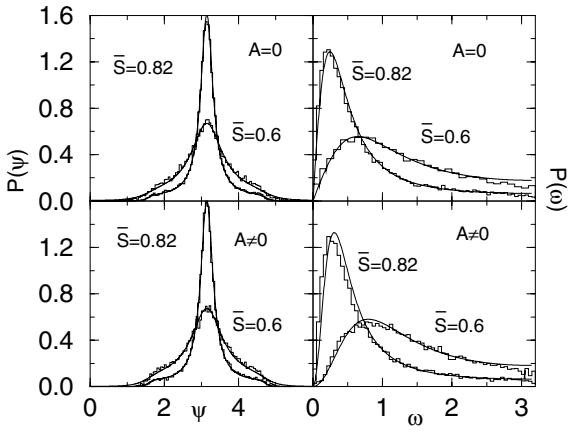

Figure 9. The $\mathcal{P}(\psi)$ and $\mathcal{P}(\omega)$ distributions for a 2×2 scattering matrix S. The solid lines correspond to the predictions of RMT (56). The upper panels correspond to $A = 0$, the lower panels to $A \neq 0$.

[35, 37, 39]. For the one-channel case it was found [37, 39] that the probability distribution of the scaled (with the mean level spacing Δ) partial delay times $T_i = \frac{\Delta}{2\pi}\frac{\partial\phi_i(k)}{\partial k}$ is

$$\mathcal{P}_{\bar{S}}^{(\beta)}(T) = \frac{\left(\frac{\beta}{2}\right)^{\beta/2}}{\Gamma\left(\frac{\beta}{2}\right)T^{2+\beta/2}} \int_0^{2\pi} \mathcal{P}(\phi)^{1+\beta/2}\, \mathrm{e}^{-\frac{\beta}{2T}\mathcal{P}(\phi)}\, \mathrm{d}\phi \tag{58}$$

where $\mathcal{P}(\phi)$ is the Poisson kernel (equation (54)). The general case of M-equivalent open channels was studied in [35, 37] where it was found that for broken time-reversal symmetry the probability distribution of partial delay times is

$$\mathcal{P}(T) = \frac{(-1)^M}{M!T^{M+2}} \frac{\partial^M}{\partial(T^{-1})^M}\left[\mathrm{e}^{-g/T} I_0\left(T^{-1}\sqrt{(g^2-1)}\right)\right] \tag{59}$$

where $I_0(x)$ stands for the modified Bessel function.

To investigate the statistical properties of the partial delay times for our system we had calculated $\mathcal{P}(T)$ for various graphs. The resulting distributions are shown in figure 10 together with the RMT predictions (58) and (59). An overall agreement is evident. Deviations appear in the short time regime (i.e. short orbits), during which the 'chaotic' component due to multiple scattering is not yet fully developed [28].

5.6. Conductance distribution

Due to the recent experimental investigation of electronic transport through mesoscopic devices [47], the study of the statistical properties of the conductance gained some importance. For a device connected to reservoirs by leads, the Landauer–Büttiker formula relates its conductance G to the transmission coefficient T_G by the expression $G = (2\mathrm{e}^2/\hbar)T_G$. When each lead supports one channel, the transmission coefficient can be written in terms of the $S^{(M)}$-matrix as

$$T_G = \sum_{i\neq j}^{M} \left|S_{i,j}^{(M)}\right|^2 = 1 - \left|S_{j,j}^{(M)}\right|^2 \tag{60}$$

where j is the input channel.

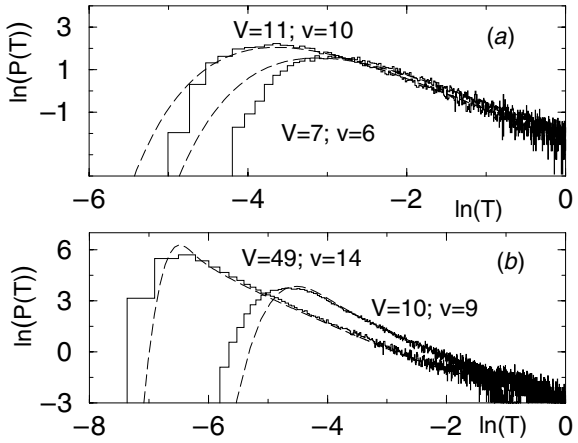

Figure 10. The distribution of the scaled partial delay times T for various graphs with Neumann boundary conditions. The dashed lines correspond to the RMT expectation (58) and (59): (*a*) One channel and $A = 0$; (*b*) $M = V$ channels and $A \neq 0$.

In the absence of direct processes, the distribution of conductance $\mathcal{P}(T_G)$ for an arbitrary number of channels was worked out within RMT, and the results describe in a satisfactory way both the numerical calculations and the experimental data (for a review see [40] and references therein). However, in the cases where direct processes appear significant, one must use Poisson's kernel (54) in its full generality. This is exactly the case with Neumann graphs since $\bar{S} \neq 0$. The probability distribution of the transmission T_G is then

$$\mathcal{P}(T_G) = \int \delta\left(T_G - \sum_{i \neq j} |S_{i,j}|^2\right) \mathcal{P}_{\bar{S}}(S)\, \mathrm{d}\mu(S). \tag{61}$$

For the case $M = 2$ and for a diagonal $\bar{S}$-matrix (only direct reflection) with equivalent channels $\bar{S}_{11} = \bar{S}_{22} = \bar{S}$, equation (61) can be worked out analytically [34] in the limit of strong reflection and $T_G \ll 1$. The resulting expression is

$$\mathcal{P}_{\beta=1}(T_G) = \frac{8}{\pi^2(1-\bar{S}^2)} T_G^{-1/2} \qquad T_G \ll (1-\bar{S}^2)^2. \tag{62}$$

For $\beta = 2$ one can compute in a closed form the whole distribution [40]

$$\mathcal{P}_{\beta=2}(T_G) = (1-\bar{S}^2)\frac{(1-\bar{S}^4)^2 + 2\bar{S}^2(1+\bar{S}^4)T_G + 4\bar{S}^4 T_G^2}{((1-\bar{S}^2)^2 + 4\bar{S}^2 T_G)^{5/2}}. \tag{63}$$

Our numerical results for a regular graph with two leads are plotted in figure 11 together with the RMT results (61), (62) and (63). Note that the small conductances are emphasized, because of the presence of direct reflection and no direct transmission. At the same time, the most pronounced differences between the two symmetry classes are for $T_G \ll 1$, where for $\beta = 1$ the conductance distribution diverges while it takes a finite value for $\beta = 2$.

6. Scattering from star graphs

So far, we have studied scattering from well-connected graphs, and we have shown that many statistical properties of the scattering matrix are described by RMT. We shall dedicate

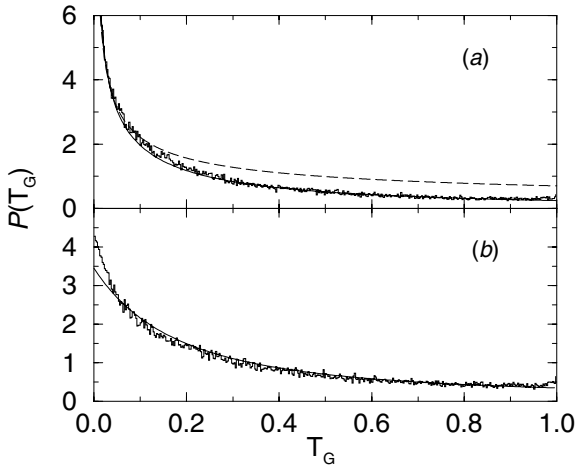

Figure 11. Conductance distribution $\mathcal{P}(T_G)$ for a graph with $M = 2$ channels. (*a*) Time-reversal symmetry is preserved ($A = 0$). The solid line is the RMT result equation (61) where we had used equation (56) for the Poisson kernel while the dashed line is the approximate expression (62). (*b*) Broken time-reversal symmetry ($A \neq 0$). The solid line is the RMT result equation (63).

this section to demonstrating the statistical properties of the S-matrix for graphs which have non-uniform connectivity.

A representative example of this category is the 'star' (or 'hydra') graphs [14, 16]. They consist of v_0 bonds, all of which emanate from a single common vertex labelled with the index $i = 0$. The vertex at $i = 0$ will be referred to in the following as the *head*. The total number of vertices for such a graph is $V = v_0 + 1$, and the vertices at the end of the bonds will be labelled by $i = 1, \ldots, v_0$. The star is a bipartite graph, a property which implies, e.g., that there exist no periodic orbits of odd period [14]. To turn a star graph into a scattering system we add a lead to its head.

It is simple to derive the scattering matrix $S = S^{(M=1)}$ for a Neumann star. It reduces to a phase factor,

$$S(k) \equiv \mathrm{e}^{\mathrm{i}\phi(k)} = \frac{-\sum_{i=1}^{v_0} \tan(kL_i) + \mathrm{i}}{\sum_{i=1}^{v_0} \tan(kL_i) + \mathrm{i}}. \tag{64}$$

The spectrum $\{k_n\}$ of the closed system can be identified as the set of wave vectors for which $S(k)$ equals 1, which implies that no current flows in the lead. The resulting quantization condition is

$$1 - S(k) = 0 \longleftrightarrow \frac{2\sum_{i=1}^{v_0} \tan(k_n L_i)}{\sum_{i=1}^{v_0} \tan(kL_i) + \mathrm{i}} = 0 \tag{65}$$

which is satisfied once $\sum_{i=1}^{v_0} \tan(k_n L_i) = 0$. This is identical with the condition derived in [14].

The poles $\{\kappa_n\}$ are the complex zeros of

$$\sum_{i=1}^{v_0} \tan(\kappa_n L_i) + \mathrm{i} = 0. \tag{66}$$

To first order in $\frac{1}{v_0}$, we get

$$\Gamma_n^{(1)} = \frac{1}{\sum_{i=1}^{v_0} \frac{L_i}{\cos(2k_n L_i)+1}} \tag{67}$$

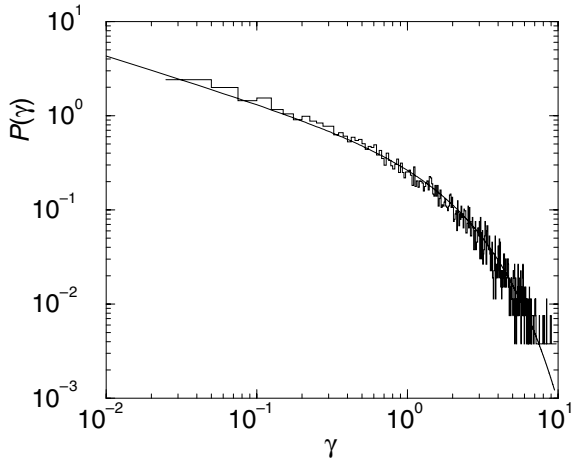

Figure 12. The rescaled resonance width distribution $\mathcal{P}(\gamma)$ for a star graph with $v_0 = 20$. The solid line is the RMT prediction equation (44).

which can be used as a starting point for the exact evaluation of the poles. For the latter one has to perform a self-consistent search for the complex zeros of the secular equation (66). This is a time-consuming process and the correct choice of the initial conditions is very important.

In figure 12, we present our numerical results for the distribution of rescaled resonance widths $\mathcal{P}(\gamma)$ for a star with $v_0 = 20$. The data are in excellent agreement with the RMT expectation given in equation (44). We point out that in this case the coupling to the continuum is weak since $g \simeq 10 \gg 1$ and therefore the χ^2 distribution with $M = 1$ is applicable.

Using equation (64) we get the following relation for the scaled delay times:

$$T(k) = \frac{\Delta}{2\pi} \frac{2\sum_{i=1}^{v_0} \frac{L_i}{\cos^2(kL_i)}}{1 + \left(\sum_{i=1}^{v_0} \tan kL_i\right)^2} \tag{68}$$

which can be used to generate $\mathcal{P}(T)$. The latter is reported in figure 13 together with the RMT prediction (59). We note that although the tail of the distribution agrees reasonably well with the RMT prediction, there are considerable deviations at the origin. Their origin is associated with the fact that stars are bipartite graphs and thus all periodic orbits are of even period. As a result the body of the distribution $\mathcal{P}(T)$ is moved towards larger delay times T.

A peculiarity of the star graph is that the mean time delay is twice as large as the expected one from semiclassical considerations. To be more specific, for a generic chaotic system coupled to M channels, one has [41]

$$\langle T \rangle_k \simeq \frac{M+1}{M} \frac{\Delta}{2\pi} \langle l_p \rangle_k \tag{69}$$

where $\langle l_p \rangle_k \simeq \Gamma_{cl}^{-1}$ is the average length of the classical paths inside the interaction area. Thus for the star with $M = 1$, we would expect based on equation (69) that $\langle T \rangle_k \simeq \frac{\Delta}{2\pi} 2\Gamma_{cl}^{-1}$. However, due to the fact that all the periodic orbits on the star graph are self-tracing we get an additional factor of 2 and thus

$$\langle T \rangle_k = \frac{\Delta}{2\pi} 4\Gamma_{cl}^{-1}. \tag{70}$$

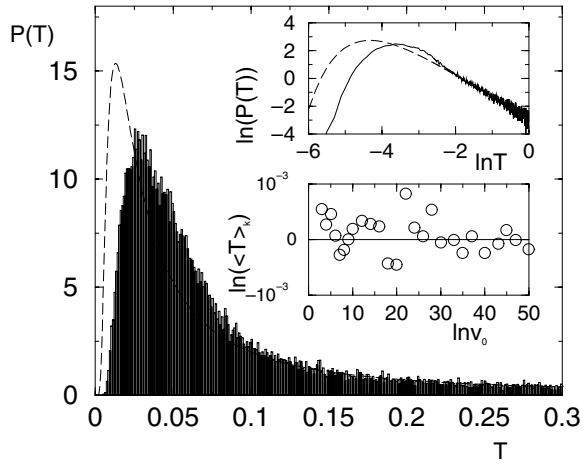

Figure 13. The distribution of the scaled partial delay times $\mathcal{P}(T)$ for a star graph with $v_0 = 20$. The dashed line is the RMT prediction equation (58). In the upper inset we show the same data in a double logarithmic plot. In the lower inset we plot the numerical results for $\langle T\rangle_k$ ($\circ$). The solid line is the asymptotic value 1 expected from semiclassical considerations.

The corresponding classical decay rate Γ_{cl} can be found exactly by a direct evaluation of the eigenvalues of the classical evolution operator $\tilde{U}$. One can easily show that

$$\tilde{U} = \begin{pmatrix} 0 & \mathbf{1} \\ (\tilde{\sigma}^{(0)})^2 & 0 \end{pmatrix} \tag{71}$$

where $\tilde{\sigma}^{(0)}$ is the $v_0 \times v_0$ vertex scattering matrix at the star head as defined in equation (5), while $\mathbf{1}$ denotes the $v_0 \times v_0$ identity matrix. The square of the classical evolution operator $\tilde{U}^2$ has a block diagonal form

$$\tilde{U}^2 = \begin{pmatrix} (\tilde{\sigma}^{(0)})^2 & 0 \\ 0 & (\tilde{\sigma}^{(0)})^2 \end{pmatrix} \tag{72}$$

and its spectrum consists of the values $1 - \frac{4}{(1+v_0)^2}$ with multiplicity 2 and $1 - \frac{4}{(1+v_0)}$ with multiplicity $2v_0 - 2$. Therefore the spectrum of $\tilde{U}$ is

$$\begin{aligned} \lambda_u &= \pm\sqrt{1 - \frac{4}{(1+v_0)^2}} \\ &= \pm\sqrt{1 - \frac{4}{1+v_0}} \qquad \text{with multiplicity } v_0 - 1. \end{aligned} \tag{73}$$

For short times where the classical evolution is applicable, the dominant eigenvalue is $\lambda_u = \sqrt{1 - \frac{4}{1+v_0}}$ leading to a classical decay rate

$$\Gamma_{cl} \simeq \frac{2}{1+v_0}. \tag{74}$$

Substituting equation (74) we get eventually that $\langle T\rangle_k = \frac{1+v_0}{v_0} \xrightarrow{v_0 \to \infty} 1$ which indicates that the mean time a particle spends inside the interaction regime is proportional to the Heisenberg time. Our numerical calculations reported in the lower inset of figure 13 agree nicely with the semiclassical prediction (70).

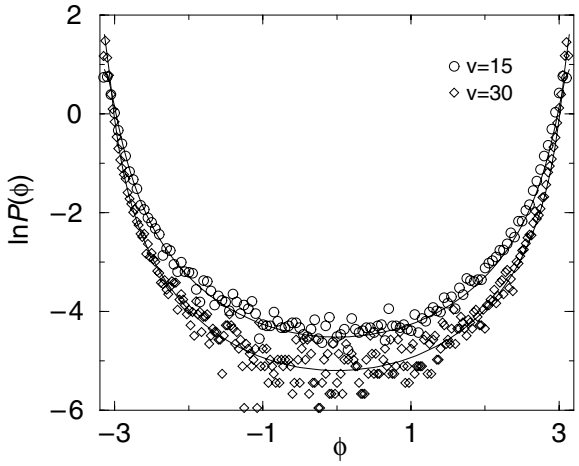

Figure 14. The distribution of phases $\mathcal{P}(\phi)$ of the S_H-matrix for two stars with $v_0 = 15$ and $v_0 = 30$. The solid lines are the corresponding theoretical predictions (77).

Finally, we analyse the distribution of S when generated over different realizations of the lengths of the bond. For the one-channel case this is equivalent to the distribution $\mathcal{P}(\phi)$ of the phase of the S-matrix. To derive the latter, it is convenient to rewrite the S-matrix in the following form:

$$S \equiv \exp(\mathrm{i}\phi) = (-K + \mathrm{i})/(K + \mathrm{i}) \tag{75}$$

with $K = \sum_{i=1}^{v} \tan(kL_i)$. The probability distribution of K is

$$\begin{aligned}\mathcal{P}(K) &= \left\langle \delta\left(K - \sum_{i=1}^{v} \tan(kL_i)\right)\right\rangle_L \\ &= \frac{1}{2\pi}\int \mathrm{e}^{\mathrm{i}Kx}\,\mathrm{d}x \left(\frac{1}{\delta L}\int_{L_{\min}}^{L_{\max}} \mathrm{d}L\,\mathrm{e}^{-\mathrm{i}x\tan(kL)}\right)^v \\ &= \frac{1}{\pi}\frac{v}{v^2 + K^2}.\end{aligned} \tag{76}$$

Thus, with $\bar{S} \equiv \langle S\rangle = \frac{1-v}{1+v}$, we get

$$\mathcal{P}(\phi) = \mathcal{P}(K)\left|\frac{\mathrm{d}K}{\mathrm{d}\phi}\right| = \frac{1}{2\pi}\frac{1-\bar{S}^2}{1+\bar{S}^2 - 2\bar{S}\cos\phi}. \tag{77}$$

Equation (77) reproduces the Poisson's kernel for a one-channel scattering matrix, derived in the framework of RMT [37]. The conditions under which this result is derived in [37] are fulfilled *exactly* in the present case. Our numerical results are reported in figure 14 and are in excellent agreement with the theoretical prediction equation (77).

7. Conclusions

In this paper, we turned quantum graphs into scattering systems. We show that they combine the desirable features of both behaving 'typically' and being mathematically simple. Thus, we propose them as a convenient tool to study the generic behaviour of chaotic scattering systems.

The classical dynamics on an open graph was defined, and the classical staying probability was shown to decay in an exponential way. The resulting classical escape rate was calculated and used to describe the properties of the corresponding quantum system. The scattering matrix was written in terms of classical orbits and an exact trace formula for the resonance density was found. A gap for the resonance widths has been obtained for 'generic' graphs and its absence was explained for Neumann graphs. An analysis of the cross-section autocorrelation function was performed and its non-universal characteristics were explained in terms of the short classical scattering trajectories. Finally, due to the relative ease with which a large number of numerical data can be computed for the graph models, we performed a detailed statistical analysis of delay times, resonance widths and distribution of the S-matrix. Our results compare well with the predictions of RMT indicating that our model can be used to understand the origin of the connection between RMT and the underlying classical chaotic dynamics.

The results reported here complete our previous investigations on graphs. We conclude that quantum graphs may serve as a convenient paradigm in the area of quantum chaos, both for spectral and scattering studies.

Acknowledgments

We acknowledge many useful discussions with Y Fyodorov and H Schanz. This work was supported by the Minerva Center for Nonlinear Physics, and an Israel Science Foundation Grant. TK acknowledges a postdoctoral fellowship from the Feinberg School, The Weizmann Institute of Science.

References

[1] Alexander S 1985 *Phys. Rev.* B **27** 1541
[2] Flesia C, Johnston R and Kunz H 1987 *Europhys. Lett.* **3** 497
[3] Mitra R and Lee S W *Analytical Techniques in the Theory of Guided Waves* (New York: Macmillan)
[4] Anderson P W 1981 *Phys. Rev.* B **23** 4828
Shapiro B 1982 *Phys. Rev. Lett.* **48** 823
[5] Chalker J T and Coddington P D 1988 *J. Phys. C: Solid State Phys.* **21** 2665
Klesse Rochus and Metzler Marcus 1997 *Phys. Rev. Lett.* **79** 721
Klesse R 1996 *PhD Thesis* Universitat zu Köln (Erfurt: AWOS-Verlag)
[6] Avishai Y and Luck J M 1992 *Phys. Rev.* B **45** 1074
Nakayama T, Yakubo K and Orbach R L 1994 *Rev. Mod. Phys.* **66** 381
[7] Imry Y 1996 *Introduction to Mesoscopic Systems* (New York: Oxford)
Kowal D, Sivan U, Entin-Wohlman O and Imry Y 1990 *Phys. Rev.* B **42** 9009
[8] Vidal J, Montambaux G and Doucot D 2000 *Phys. Rev.* B **62** R16294
[9] Zhang Z Q *et al* 1998 *Phys. Rev. Lett.* **81** 5540
[10] de Verdière C 1998 *Spectres de Graphes* (Marseille: Société Mathématique de France)
[11] Exner P 1995 *Phys. Rev. Lett.* **74** 3503
Exner P and Seba P 1989 *Rep. Math. Phys.* **28** 7
Avron J E, Exner P and Last Y 1994 *Phys. Rev. Lett.* **72** 896
Carlson R 1998 *Electron. J. Diff. Eqs* **6** 1
[12] Roth J-P 1984 *Lecture Notes in Mathematics: Theorie du Potentiel* ed A Dold and B Eckmann (Berlin: Springer) pp 521–39
[13] Kottos T and Smilansky U 1997 *Phys. Rev. Lett.* **79** 4794
[14] Kottos T and Smilansky U 1999 *Ann. Phys., NY* **274** 76
[15] Akkermans E, Comtet A, Desbois J, Montambaux G and Texier C 2000 *Ann. Phys., NY* **284** 10
[16] Berkolaiko G and Keating J 1999 *J. Phys. A: Math. Gen.* **32** 7827
Berkolaiko G, Bogomolny E B and Keating 2001 *J. Phys. A: Math. Gen.* **34** 335

[17] Schanz H and Smilansky U 2000 *Phys. Rev. Lett.* **84** 1427
Schanz H and Smilansky U 1999 *Proc. Australian Summer School on Quantum Chaos and Mesoscopics (Canberra, Australia, 1999)* (*Preprint* chao-dyn/9904007)
Kottos T and Schanz H 2001 *Physica* E **9** 523
[18] Tanner G 2001 *J. Phys. A: Math. Gen.* **33** 3567
[19] Berkolaiko G, Schanz H and Whitney R S 2002 *Phys. Rev. Lett.* **88** 104101
[20] Barra F and Gaspard P 2000 *J. Stat. Phys.* **101** 283
Barra F and Gaspard P 2001 *Phys. Rev.* E **63** 066215
[21] Kaplan L 2001 *Phys. Rev.* E **64** 036225
Kottos T 2002 in preparation
[22] Kottos T and Smilansky U 2000 *Phys. Rev. Lett.* **85** 968
[23] Barra F and Gaspard P 2002 *Phys. Rev.* E **65** 016205
[24] Texier C and Montambaux G 2001 *J. Phys. A: Math. Gen.* **34** 10307
Texier C 2002 *J. Phys. A: Math. Gen.* **35** 3389
[25] Miller W H 1974 *Adv. Chem. Phys.* **25** 69
[26] Smilansky U 1989 *Les Houches Summer School on Chaos and Quantum Physics* ed M-J Giannoni *et al* (Amsterdam: North-Holland) pp 371–441
See also Akkermans E *et al* (ed) 1994 *Les Houches Summer School on Mesoscopic Quantum Physics* (Amsterdam: North-Holland) pp 373–433
[27] Gaspard P 1991 *Quantum Chaos: Proc. E Fermi Summer School 1991* ed G Casati *et al* (Amsterdam: North-Holland) p 307
Gaspard P and Rice S A 1989 *J. Chem. Phys.* **90** 2225, 2242, 2255
Gaspard P and Rice S A 1989 *J. Chem. Phys.* **91** E3279
[28] Blümel R and Smilansky U 1990 *Phys. Rev. Lett.* **64** 241
[29] Eckhardt B, Varga I and Pollner P 2001 *Physica* E **9** 535
[30] Moldauer P A 1975 *Phys. Rev.* C **11** 426
Moldauer P A 1967 *Phys. Rep.* **157** 907
Simonius M 1974 *Phys. Lett.* B **52** 279
[31] Mello P, Pereyra P and Seligman T H 1985 *Ann. Phys., NY* **161** 254
[32] Jalabert R A, Stone A D and Alhassid Y 1992 *Phys. Rev. Lett.* **68** 3468
[33] Haake F, Izrailev F, Lehmann N, Saher D and Sommers H-J 1992 *Z. Phys.* B **88** 359
Lehmann N, Saher D, Sokolov V and Sommers H-J 1995 *Nucl. Phys.* A **582** 223
[34] Brouwer P W and Beenakker C W J 1994 *Phys. Rev.* B **50** 11263
[35] Fyodorov Y V and Sommers H-J 1996 *Phys. Rev. Lett.* **76** 4709
Fyodorov Y V, Savin D V and Sommers H-J 1997 *Phys. Rev.* E **55** R4857
[36] Sommers H-J, Fyodorov Y V and Titov M 1999 *J. Phys. A: Math. Gen.* **32** L77
Fyodorov Y and Sommers H-J 1996 *Pis. Zh. Eksp. Teor. Fiz.* **63** 970
Fyodorov Y and Sommers H-J 1996 *JETP Lett.* **63** 1026
[37] Fyodorov Y and Sommers H-J 1997 *J. Math. Phys.* **38** 1918
Mello P 1994 *Les Houches Summer School on Chaos and Quantum Physics* ed E Akkermans *et al* (Amsterdam: North-Holland) pp 437–91
[38] Brouwer P W, Frahm K M and Beenakker C W 1997 *Phys. Rev. Lett.* **78** 4737
[39] Gopar V A and Mello P 1998 *Europhys. Lett.* **42** 131
[40] Mello P A and Baranger H U 1999 *Waves Random Media* **9** 105
[41] Doron E and Smilansky U 1992 *Nonlinearity* **5** 1055
Doron E and Smilansky U 1992 *Phys. Rev. Lett.* **68** 1255
[42] Mahaux C and Weidenmuller H A 1969 *Shell Model Approach in Nuclear Reactions* (Amsterdam: North-Holland)
[43] Birman M Sh and Yafaev D R 1993 The spectral shift function. The work of M G Krein and its further development *St Petersburg Math. J.* **4** 833–70
[44] Sokolov V and Zelevinsky G 1988 *Phys. Lett.* B **202** 10
Sobeslavsky E, Dittes F M and Rotter I 1995 *J. Phys. A: Math. Gen.* **28** 2963
[45] Ericson T 1960 *Phys. Rev. Lett.* **5** 430
Ericson T 1963 *Ann. Phys., NY* **23** 390
[46] Verbaarschot J J M, Weidenmüller H A and Zirnbauer M R 1985 *Phys. Rep.* **129** 367
Verbaarschot J J M 1986 *Ann. Phys., NY* **168** 368
[47] Marcus C M, Rimberg A J, Westervelt R M, Hopkins P F and Gossard A C 1992 *Phys. Rev. Lett.* **69** 506